The Dependence of Electromagnetic Energy Absorption upon Human-Head Modeling at 1800 MHz

Klaus Meier, *Associate Member, IEEE,* Volker Hombach, *Member, IEEE,* Ralf Kästle, Roger Yew-Siow Tay, *Member, IEEE,* and Niels Kuster, *Member, IEEE*

***Abstract*— The authors of a previously published paper on the dependence of electromagnetic (EM) energy absorption concluded that homogeneous modeling of the human head is suited for assessing the spatial-peak absorption for transmitters operating at 900 MHz or below. Additional studies became necessary for the frequency bands utilized by new mobile communications systems (i.e., 1.5 and 2.5 GHz) since some peripheral tissue layers have a thickness of the range of $\lambda/4$–$\lambda/2$. The results of the simulations combined with worst-case considerations confirmed the anticipated and more complex relationship between absorption and anatomical details at these higher frequencies. Nevertheless, a homogeneous representation of the head is suited for assessing the maximum specific absorption rate (SAR) in the head of the user of mobile telecommunication equipment (MTE) if the appropriate dielectric parameters are chosen.**

I. Introduction

SINCE the beginning of 1997, the U.S. Federal Communications Commission (FCC) requires the routine specific absorption rate (SAR) evaluation of mobile telecommunications devices prior to equipment authorization or use [1]. Similar recommendations have been made by other standardization bodies [2]. These exposure limits are defined in terms of the SAR $(\mathrm{SAR} = \sigma E^2/\rho)$ averaged either over 1 or 10 g of tissue mass.

Two dosimetric E-field scanning systems have been developed for such compliance tests [3], [4], both of which are restricted to measurements in shell phantoms filled with a tissue-simulating liquid, the recipes for which are given in [5]. The suitability of such homogeneous head phantoms has been investigated for the 900-MHz frequency band [5]. The results of this study, which was conducted using several head phantoms of varying complexity, showed that the assessed spatial-peak SAR is always higher in homogeneous head phantoms than in nonhomogeneous phantoms. Most important is the finding that the overestimation for the region above the ear is quite moderate, i.e., less than 10% for an averaging mass of 10 g and less than 25% for 1 g. On the basis of the energy absorption mechanism [6], these findings can be extended to frequencies as low as 300 MHz. However, an extension to higher frequencies was not possible without further studies, since peripheral tissue layers are expected to play a more prominent role than at lower frequencies. In the frequency bands of the new-generation cellular-phone systems, i.e., between 1.5–2.5 GHz, the thickness of some tissue layers are in the range of $\lambda/4$–$\lambda/2$, whereby the attenuation in these layers is not significant enough to exclude possible enhancement effects due to reflection at the boundaries or due to matching effects.

The objective of this paper is to assess these effects with respect to the suitability of using homogeneous phantoms for testing compliance of mobile telecommunication equipment (MTE) at these frequencies. The methods and the approaches adopted are basically analogous to those for the study at 900 MHz in [7], but performed at 1800 MHz.

A. Numerical and Experimental Techniques

The numerical analysis of the complex head phantoms were performed with the commercial software package MAFIA. This code based on the finite-integration technique (FIT) [8] is slightly conceptually different to the finite-difference time-domain (FDTD) technique, but nevertheless results in the same numerical scheme. The open domains were bounded by second-order Mur absorbing-boundary conditions. Excitation was accomplished using a smoothly increasing harmonic function and the computation was terminated after steady state was reached (usually after 10–20 periods).

For the spherical phantoms, the three-dimensional (3-D) multiple multipole (MMP) software package was used. This frequency-domain boundary technique enables reliable error estimations and is especially efficient and accurate for layer spheres [9].

The dosimetric assessment system (DASY2) was used to experimentally evaluate the absorbed electromagnetic (EM) power inside the different shell phantoms [4]. The uncertainty for compliance testing was assessed to be within $\pm 25\%$ [10].

B. Head Phantoms

The four different complex numerical head phantoms $M1$–$M4$ are described in [7]. $M1$–$M3$ are based on MRI scans of three different adults, each varying considerably in size and shape. Thirteen different tissue types were

Manuscript received August 1996; revised March 1997.

K. Meier, R. Kästle, and N. Kuster are with the Swiss Federal Institute of Technology (ETH), CH-8092 Zurich, Switzerland.

V. Hombach is with Deutsche Telekom, Technologiezentrum, Darmstadt, Germany.

R. Y.-S. Tay is with Motorola Inc., Florida Corporate Electromagnetic Research Laboratory, Plantation, FL 33322 USA.

Publisher Item Identifier S 0018-9480(97)08024-1.

TABLE I
TISSUE PARAMETERS OF THE NUMERICAL MODELS AT 1800 MHz

Tissue	ref. [11]		ref. [12]	
	ϵ_r	σ [mho/m]	ρ [kg/m^3]	λ [mm]
bone (M1, M2, M3, M4)	19.7	0.55	1850	37
cartilage (M1, M2, M3)	38.3	1.23	1000	27
skin (M1, M2, M3, M4)	38.4	0.99	1100	27
fat (M1, M2, M3)	9.4	0.25	1100	54
muscle (M1, M2, M3, M4)	55.2	1.30	1040	22
brain, grey matter (M1, M2)	51.5	1.57	1030	23
brain, white matter (M1, M2)	33.1	0.84	1030	29
brain, experiments (M3, M4)	41.0	1.65	1030	26
CSF (M1, M2, M3)	77.8	2.83	1000	19
aqueous humour (M1 – M4)	67.2	2.08	1010	20
eye lens nucleus (M1, M2, M3)	34.7	0.87	1050	28
eye lens outer (M1, M2, M3)	49.5	1.33	1050	24
eye sclera (M1, M2, M3)	52.7	1.67	1020	23
blood (M3)	54.0	2.27	1060	22
parotid gland (M3)	70.0	1.90	1000	20

distinguished for which the electrical parameters given in Table I were assigned. The voxel size varied between 1 mm^3 to 12 mm^3, depending on the source of the data. The fourth phantom $M4$ corresponds to the most complex experimental phantom $E1$ (five-tissue phantom), which was discretized based on MRI and CT scans. In addition to the nonhomogeneous modeling, the internal tissue distribution was simplified. In the first step, the parameters of average brain tissue were assigned to all tissues except the bone structure. These phantoms are referred to in the following as *simplified* phantoms. Finally, the bone tissue was also replaced by brain-average tissue (referred to as *homogeneous* phantoms).

The three experimental phantoms are also described in detail in [7]. The experimental phantom $E1$ is commercially available and simulates five tissue types: skin, muscle, bone, eyes, and brain. The electrical parameters of which are given in Table II. Brain was simulated by a sugar-water solution having the electrical parameters $\epsilon_r = 41 \pm 5\%$ and $\sigma = 1.69 \pm 6\%$ mho/m. The second model $E2$ is a polyester shell copy of $E1$, and the third model $E3$ is a fiberglass-shell phantom currently used in various laboratories in the USA and Europe for compliance tests. Both $E2$ and $E3$ were filled with the same tissue simulating liquid as $E1$.

In order to avoid the uncertainties inherent in modeling actual handsets, a dipole of 0.45λ in length was chosen. It was positioned at a distance of 15 mm from the head and oriented parallel to the body's axis, as shown in Fig. 1. In the numerical approach, the dipole was simulated as a filament 0.45λ in length. An 1800-MHz dipole of exactly the same length and made of standard 2.2-mm semirigid coaxial cable was used for the measurements. The dipole is constructed the same way as described in [7], enabling accurate measurement

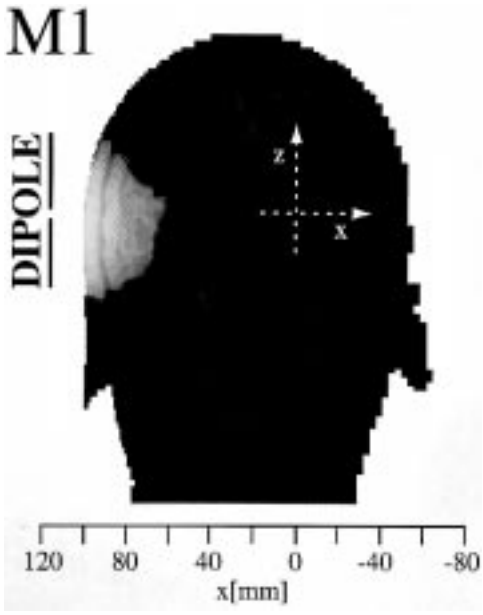

Fig. 1. SAR distribution in the xz-plane of head phantom $M1$ (for quantitative values see Fig. 2).

TABLE II
TISSUE PARAMETERS OF THE EXPERIMENTAL MODELS AT 1800 MHz

Tissue	ref. [11]		ref. [12]	
	ϵ_r	σ [mho/m]	ρ [kg/m^3]	λ [mm]
bone (E1)	13.4	0.30	1850	45
skin (E1)	32.5	1.98	1100	28
muscle (E1)	50.6	1.56	1040	23
brain, experiments (E1 – E3)	41.0	1.65	1030	26
eye (E1)	67.6	2.26	1030	20

of the feedpoint impedance. All results shown in the following were normalized to an antenna feedpoint current of 100 mA, which approximately corresponded to antenna input power of 0.38—0.48 W, depending on the modeling of the head.

II. RESULTS AND DISCUSSION

Fig. 1 shows the SAR distribution in the cross section of the 13-tissue phantom $M1$ (voxel size 1 mm^3). The qualitative SAR distributions in the other phantoms were very similar. More information can be derived from Figs. 2 to 4, in which the SAR values on the x-axis of the different phantoms are compared. The x-axis intersects the body's axis and the feedpoint of the dipole which is oriented in z-direction and is located at $x = 115$ mm. The distance between dipole and skin is 15 mm, i.e., surface of the skin is at $x = 100$ mm.

At 1800 MHz, most of the induced fields are already absorbed in the peripheral skin–muscle layer compared to 900 MHz because the penetration depth is reduced by about 50%. Hence, the second maximum at the brain layer is much less pronounced than at lower frequencies. The values at the surface are nearly twice as large as those at 900 MHz, which

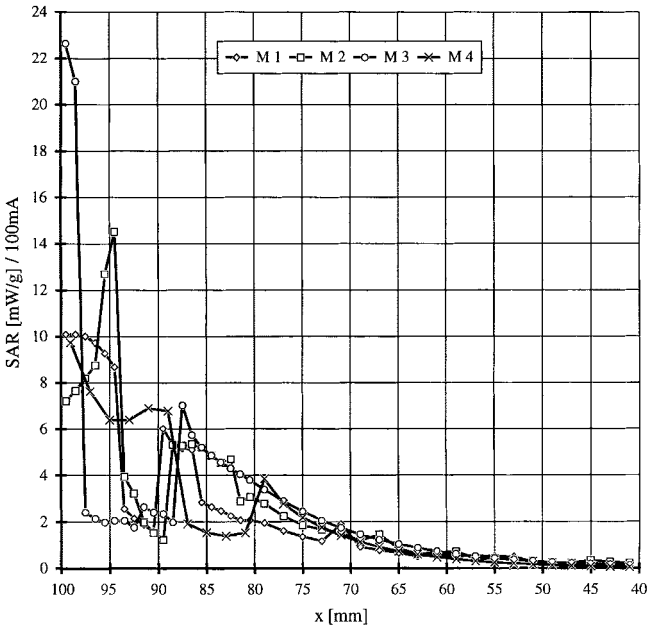

Fig. 2. SAR profile in the complex head models ($M1$–$M4$) at 1.8 GHz above the antenna feedpoint.

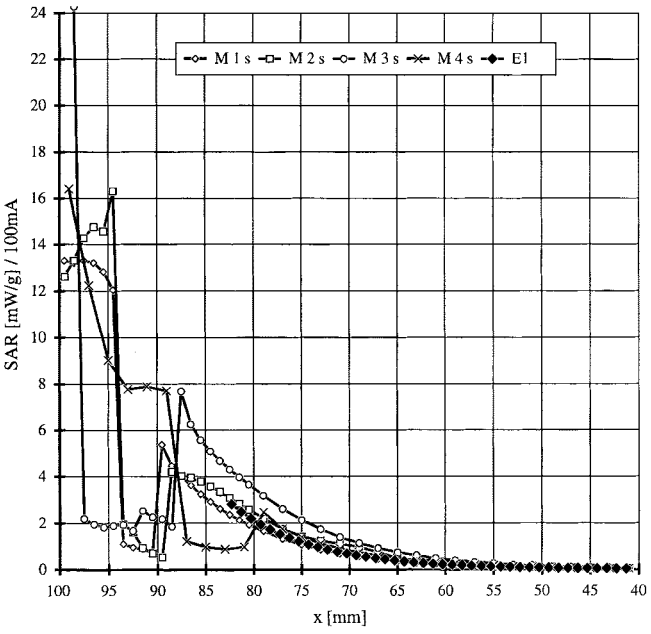

Fig. 3. SAR profile in the simplified head models ($M1$–$M4$) at 1.8 GHz above the antenna feedpoint. All tissues except the bone tissue were substituted with $\epsilon_r = 41$, $\sigma = 1.65$ mho/m.

tallies well with the approximation formula given in [6]. The determining factors are the greater conductivity and, more importantly, the decreased coupling due to the larger distance of the dipole in terms of wavelength (i.e., larger value of the correction factor in [6]).

The pattern of the SAR distribution within the single layers greatly deviates from the strongly monotonous decay observed at lower frequencies (i.e., is not approximately proportional to σH_{inc}^2). The reason is that the thickness of some tissue layers is in the order of $\lambda/4$–$\lambda/2$ (see Table I), which causes effects similar to standing waves and the impedance-matching effects

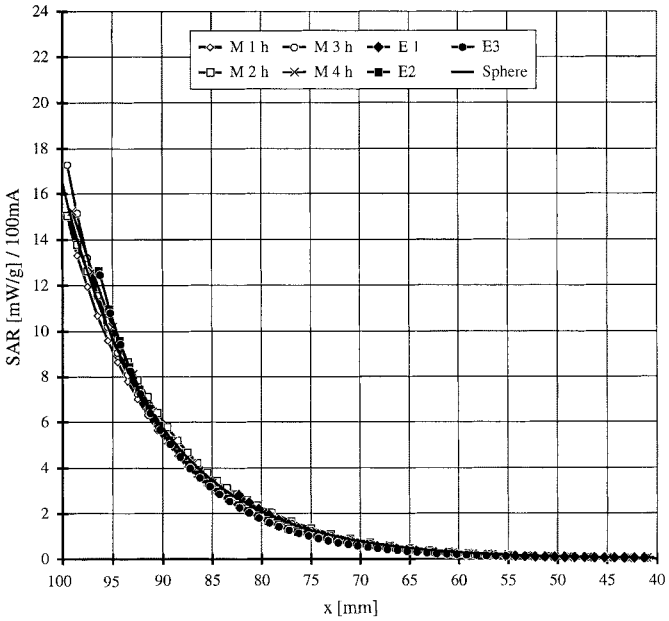

Fig. 4. SAR profile in the homogeneous head models ($M1$–$M4$), the sphere and the experimental models ($E1$–$E3$) at 1.8 GHz above the antenna feedpoint. The tissue parameters were $\epsilon_r = 41$, $\sigma = 1.65$ mho/m.

of layered bodies exposed to an incident plane wave [13]. The most pronounced effects occur inside the extraordinarily thick skin layer of phantom $M4$, which is nearly $\lambda/2$ (see Fig. 2).

Any differences in the SAR distribution disappear as expected in the case of homogeneous modeling of the various phantoms. The value at the surface also tallies well with the 17 mW/g estimated by the approximation formula in [6].

The volume-averaged SAR^V values ($\text{SAR}^V = \sigma E^2$) are compared in Figs. 5 and 6. The 10 cm^3-averaged values are about 5% higher than those from the heterogeneous phantoms. In the case of the 1-cm^3 averaging volume, the homogeneous numerical results as well as the experimental results are 20% higher. The main reason for these rather large differences lies in the significant differences in conductivity between skin ($\sigma = 0.99$ mho/m) and the material used in the simplified and homogeneous phantoms ($\sigma = 1.65$ mho/m).

Regarding compliance testing, it is important to note that specific tissue layers in the head may not only increase the local SAR values but also the spatial-peak SAR values (see Figs. 5 and 6). In order to verify these findings and to assess the greatest possible enhancements due to standing-wave and matching effects, additional studies were performed.

First the phenomena observed were verified in spherical models using equivalent layer configurations as found on the x-axis in the complex models. The computations were performed with 3-D MMP; the uncertainties of the result were assessed by result validation procedures to be less than $\pm 1\%$. Some results are shown in Fig. 7. The comparison shows the same qualitative and quantitative distributions in the homogeneous sphere with all homogeneous numerical and experimental phantoms. Also, the distribution of the sphere with 10-mm skin layer and 5-mm bone layer hardly differs from that of $M4$ (see Fig. 2). An even more pronounced matching effect is found with just a 10-mm-thick bone layer.

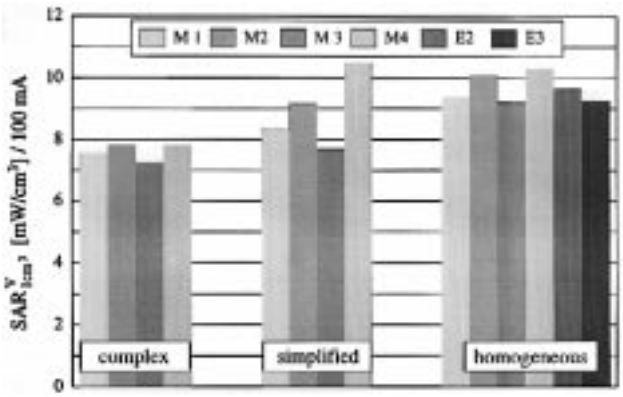

Fig. 5. Spatial-peak SAR^V values averaged over 1 cm^3 brain tissue at 1.8 GHz.

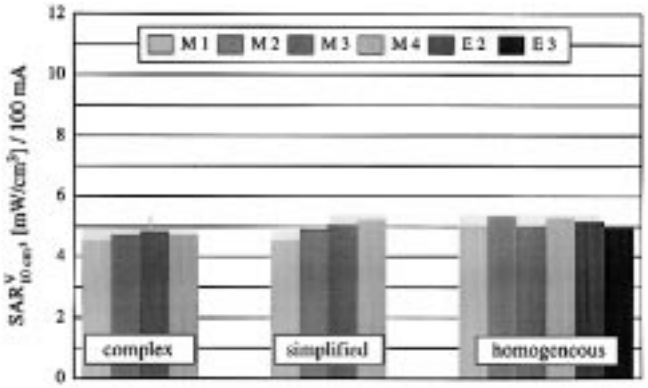

Fig. 6. Spatial-peak SAR^V values averaged over 10 cm^3 brain tissue at 1.8 GHz.

Since these effects are greatest for a planar layered structure exposed to normally oriented plane waves, the plane model was used to evaluate the worst-case enhancement with respect to the spatial-peak SAR values. The thickness of the front layers were varied in order to find the greatest enhancement compared to the homogeneous half-space ($\epsilon_r = 41, \sigma = 1.65$ mho/m). The maximum enhancement factors (EF's) found at layer thickness (d_{layer}) are shown in Table III for the different structures: skin–muscle, skin–bone, muscle–bone, and bone–brain. The parameters of Table I were used.

The enhancement effects observed in the case of the structure bone–brain vanish if the bone layer is covered by a skin layer that is thicker than 1 mm. Hence, it can be concluded that a homogeneous phantom consisting of material with the parameters ($\epsilon_r = 41, \sigma = 1.65$ mho/m) overestimates the exposure of nonhomogeneous modeling.

III. Conclusions

In the frequency bands of the new-generation cellular systems, i.e., 1.5–2.5 GHz anatomical layered-structure models of the human head can lead to increased absorption in the layers. However, the spatial-peak SAR assessed by a homogeneous phantom with the parameters of grey brain tissue are unlikely to be less than the actual SAR value induced among all potential users and under all operational conditions, i.e., it would satisfy the worst-case criteria of [14]. The overestimation is less than 5% for the 10-g averaged spatial-peak SAR and significantly less than 20% for the 1-g averaged value. In other words, homogeneous modeling of the human head is well suited for testing compliance of hand-held MTE with safety limits from 300 MHz to 2.5 GHz. The fact that these findings can also be extended to children has been demonstrated in a recently completed study [15].

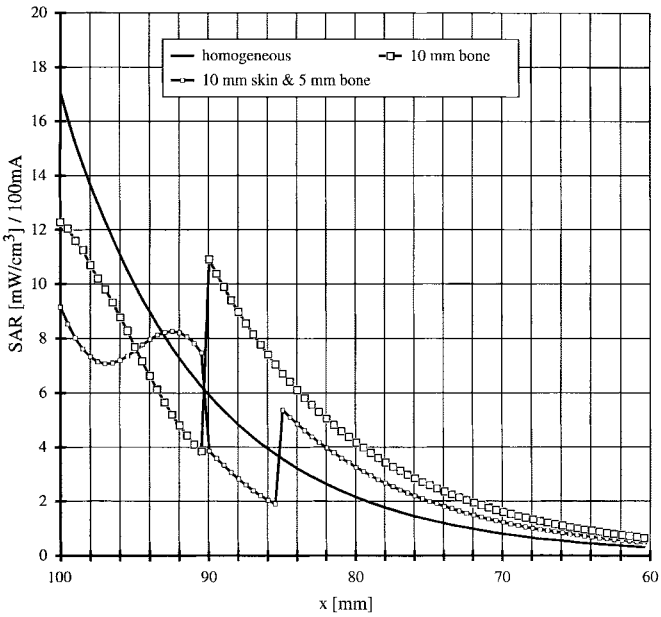

Fig. 7. Influence of a peripheral bone and skin layers on the absorption. Computed with layered spherical models at 1.8 GHz. Dipole distance is 15 mm. Outer diameter of the sphere is 200 mm.

TABLE III
Maximum EF's

Structure		SAR_{1g-avg}		$\mathrm{SAR}_{10g-avg}$	
layer	bulk	EF	d_{layer}	EF	d_{layer}
skin	muscle	0.87	7 mm	0.98	7 mm
skin	bone	0.85	14 mm	none[a]	
muscle	bone	0.87	11 mm	none[a]	
bone	brain	1.1	7 mm	1.41	9 mm

[a]No enhancement occurs due to the lower reflection of bone tissue and the larger averaging volume.

References

[1] Federal Communications Commission, "Report and order: Guidelines for evaluating the environmental effects of radiofrequency radiation," FCC, Washington, DC, Tech. Rep. FCC 96-326 20554, 1996.
[2] N. Kuster, Q. Balzano, and J. C. Lin, Eds., *Mobile Communications Safety*. London, U.K.: Chapman & Hall, 1997.
[3] Q. Balzano, O. Garay, and T. J. Manning, "Electromagnetic energy exposure of simulated users of portable cellular telephones," *IEEE Trans. Veh. Technol.*, vol. 44, pp. 390–403, Aug. 1995.
[4] T. Schmid, O. Egger, and N. Kuster, "Automated E-field scanning system for dosimetric assessments," *IEEE Trans. Microwave Theory Tech.*, vol. 44, pp. 105–113, Jan. 1996.

[5] K. Meier, M. Burkhardt, T. Schmid, and N. Kuster, "Broad-band calibration of E-field probes in lossy media," *IEEE Trans. Microwave Theory Tech.*, vol. 44, pp. 1954–1962, Oct. 1996.
[6] N. Kuster and Q. Balzano, "Energy absorption mechanism by biological bodies in the near field of dipole antennas above 300 MHz," *IEEE Trans. Veh. Technol.*, vol. 41, pp. 17–23, Feb. 1992.
[7] V. Hombach, K. Meier, M. Burkhardt, E. Kühn, and N. Kuster, "The dependence of EM energy absorption upon human head modeling at 900 MHz," *IEEE Trans. Microwave Theory Tech.*, vol. 44, pp. 1865–1873, Oct. 1996.
[8] CST, *The MAFIA Collaboration, User's Guide Mafia Version 3.x*, CST GmbH, D 64289 Darmstadt, Germany, 1994.
[9] N. Kuster, "Multiple multipole method for simulating EM problems involving biological bodies," *IEEE Trans. Biomed. Eng.*, vol. 40, pp. 611–620, July 1993.
[10] N. Kuster, R. Kästle and T. Schmid, "Dosimetric evaluation of mobile communications equipment with known precision," *IEICE Trans. Commun.*, vol. 80-B, pps. 645–652, May 1997.
[11] Microwave Consultants, "Dielectric database," *Microwave Consultants Ltd.* London, U.K., 1994, pp. 1–5.
[12] Michael A. Jensen and Yahya Rahmat-Samii, "EM interaction of handset antennas and a human in personal communications," *Proc. IEEE*, vol. 83, pp. 7–17, Jan. 1995.
[13] C. M. Weil, "Absorption characteristics of multilayered sphere models exposed to UHF/Microwave radiation," *IEEE Trans. Biomed. Eng.*, vol. BME-22, pp. 468–476, Nov. 1975.
[14] WGMTE of CENELEC TC211/B, *Third Draft: Safety Considerations for Human Exposure to Electromagnetic Fields from Mobile Telecommunication Equipment (MTE) in the Frequency Range 30 MHz–6 GHZ*. Brussels, France: CENELEC, 1996.
[15] F. Schönborn, M. Burkhardt, and N. Kuster, "The difference of EM energy absorption between adults and children," *Health Physics*, to be published.

Klaus Meier (S'94–A'96), was born in Austria, in March 1965. He received the Diploma degree in electrical engineering from the Swiss Federal Institute of Technology (ETH), Zurich, Switzerland, in 1991, and is currently working toward the Ph.D. degree.

In 1991, he joined the ETH Institute for Electromagnetic Fields and Microwave Electronics. Since 1992, he has also been involved in the development of the dosimetric assessment system DASY. He is a co-founder of Schmid & Partner Engineering AG.

Volker Hombach (M'76), received the Dipl.-Ing. degree in electrical engineering from RWTH, Aachen, Germany, in 1975, and the Dr.-Ing. degree from the Ruhr-Universität, Bochum, Germany in 1981.

Since 1981, he has been with the Forschungszentrum of Deutsche Telekom, Darmstadt, Germany. He has been involved in the research of diffraction effects and the design and optimization of reflector antennas and feeds. His current interests include electromagnetic scattering and absorption, electromagnetic compatibility, and electromagnetic radiation hazard protection.

Dr. Hombach is a member of the German Society in Information Technology (ITG). He received the ITG Award in 1989.

Ralf Kästle was born in Tübingen, Germany, in September 1962. He received the Diploma degree in physics from the Albert-Ludwigs-University Freiburg/-Breisgau, Germany, and the Ph.D. degree in physics from the Swiss Federal Institute of Technology (ETH), Zurich, Switzerland, in 1991.

In 1991, he joined the Institute of Quantum Electronics, Swiss Federal Institute of Technology (ETH), Zurich, Switzerland, where he worked on the development of a photoacoustic setup for accurate temperature-dependent absorption measurements, as well as on theoretical aspects of the generation of acoustic waves by infrared-laser radiation. In August 1995, he joined the Institute of Electromagnetic Fields and Microwave Electronics, ETH, where he has been mainly involved in dosimetric investigations and phantom development.

Roger Yew-Siow Tay (S'82–M'86) was born in Johor Baru, Malaysia, in 1958. He received the B.S. and M.S. degrees in electrical engineering from the University of Massachusetts at Lowell, in 1983 and 1985, respectively, and the Ph.D. degree from the Swiss Federal Institute of Technology (ETH), Zurich, Switzerland, in 1997.

Upon returning from the Far East, he joined the Research and Development Department, Motorola Electronics Pte. Ltd., Singapore. In 1990, he was transferred to the Electromagnetics Laboratory, Motorola Inc., Fort Lauderdale, FL. In 1993, he was invited as an Academic Guest to the ETH for an eight-month period. He is currently a Senior Staff Engineer with the Motorola Corporate Electromagnetic Research Laboratory, Fort Lauderdale, FL. He has contributed papers in journals and conferences, and holds three patents with four patents pending.

Dr. Tay is a member of the IEEE Antennas and Propagation and IEEE Electromagnetics Compatibility Societies.

Niels Kuster (M'93) was born in Olten, Switzerland, in June 1957. He received the Diploma and Ph.D. degrees in electrical engineering from the Swiss Federal Institute of Technology (ETH), Zurich, Switzerland.

IN 1985, he joined the Electromagnetics Laboratory, ETH, where he was involved in the research and development of the generalized multipole technique (GMT), and the 3-D MMP code. In 1992, he was an Invited Professor at Motorola Inc., Fort Lauderdale, FL, for a trimester. He is currently a Professor in the Department of Electrical Engineering, ETH. His research interests include all aspects of numerical techniques in electrodynamics, near-filed measurement techniques, antenna design and biological effects of electromagnetic fields.

Dr. Kuster is a member of various scientific societies and an official member of URSI Commission K.